JOURNAL OF GEOPHYSICAL RESEARCH, VOL. 105, NO. A7, PAGES 15,715–15,727, JULY 1, 2000

Fermi acceleration of suprathermal solar wind oxygen ions

T. J. Freeman

Space Sciences Laboratory, University of California, Berkeley

G. K. Parks

Geophysics Program, University of Washington, Seattle

Abstract. The Wind spacecraft has observed numerous sunward bursts of ≈2 MeV ions upstream of the Earth's bow shock. These energetic particles are not protons or alpha particles and are probably oxygen ions. The bursts typically last several minutes at the highest energies, but they can last for tens of minutes at intermediate energies (tens to hundreds of keV). In this paper, Wind observations of the November 30, 1994, bursts and numerical particle simulations are presented that demonstrate that suprathermal solar wind O^{6+} ions, which have undergone Fermi acceleration between the bow shock and interplanetary magnetic field (IMF) rotations, are the most likely source of these bursts. Each burst either coincides with or is closely followed by a large IMF rotation. By using measured magnetic field data the timing of the bursts detected by Wind is reproduced in the simulation. Simulated spectra of H^+, He^{2+}, and O^{6+} fluxes fit the observed spectra, assuming an increase of ∼2 orders of magnitude in the high-energy tail of the solar wind oxygen distribution, relative to the average solar wind abundance of oxygen. Such enhancements in CNO group ions above 40 keV/nucleon were measured by the Suprathermal and Energetic Particle (STEP) instrument during this interval. This study concludes by predicting that ion composition and charge state measurements will show these bursts to be solar wind oxygen ions in high charge states.

1. Introduction

Observations of suprathermal upstream ions that originate at the Earth's bow shock were first reported by *Asbridge et al.* [1968]. Since then, a number of other satellites have made more detailed observations, finding the flux of suprathermal particles to be present whenever the spacecraft have been magnetically connected to the shock [*Lin et al.*, 1974]. Suprathermal ions are not restricted to the immediate vicinity of the bow shock and have been observed as far upstream as the L1 libration point [*Anderson*, 1981]. The Wind satellite has now extended the energy range of observed upstream ions to ≈2 MeV [*Skoug et al.*, 1996].

There are two competing hypotheses that have been offered to explain the origin of these suprathermal ions: Fermi acceleration and magnetospheric escape. In the Fermi model, particles gain energy through reflections between the bow shock and turbulence in the upstream region [*Terasawa*, 1979; *Eichler*, 1981; *Lee*, 1982; *Ellison*, 1985]. These models employ solutions of the diffusion equation under different assumptions about upstream turbulence. The seed population for this process is probably generated within the shock itself, where a small fraction of incident ions interacts with the wave electric field for a sufficient length of time to reach keV energies [*Scholer et al.*, 1998; *Ashford*, 1998].

In the magnetospheric escape model, ring current particles that are accelerated in the magnetosphere drift to the magnetopause and escape along magnetic field lines that connect the magnetopause to the bow shock [*Anagnostopoulos et al.*, 1986; *Sarris et al.*, 1987; *Baker et al.*, 1988; *Sibeck et al.*, 1988; *Kudela et al.*, 1990]. The general line of evidence put forth in these studies relies upon the coincidence between ion bursts in the upstream region and bursts in the magnetosheath and plasma sheet and upon spectral characteristics of the bursts. This process has been specifically modeled for the November 30, 1994, events by *Winglee et al.* [1996]. It explains the broad time-profile intermediate energy fluxes but not the sharp ≈2 MeV bursts. In contrast to hypothesizing a sole mechanism, some authors have analyzed events that appear to contain both Fermi-accelerated particles and magnetospheric particles [*Scholer et al.*, 1981; *Möbius et al.*, 1986].

Even though some observers had reported integrated energy spectra extending to ≈1 MeV prior to the launch of Wind [*Anagnostopoulos et al.*, 1986], the modeling of

Paper number 1999JA900501.
0148-0227/00/1999JA900501$09.00

upstream ion bursts was generally limited to particles of several hundred keV, assumed to be protons. This has changed with the Wind observations of ≈2 MeV ions. While ions of MeV energy can certainly escape from the magnetosphere, new requirements must be placed on Fermi acceleration models. Previous models of Fermi acceleration are capable of producing protons up to ≈300 keV, and such a cutoff was often cited as an important feature of these diffusive models [*Ellison*, 1985; *Scholer et al.*, 1990].

In this study a new model is presented. By using measured interplanetary magnetic field (IMF) data and a realistic three-dimensional bow shock model a detailed calculation of Fermi acceleration is found to reproduce the essential features in the Wind data. The model is capable of explaining the November 30, 1994, ≈2 MeV events as Fermi-accelerated solar wind oxygen ions. When applied to solar wind protons and alpha particles, the model shows that these species are not accelerated to MeV energies. The observed spectra can be explained as a combination of Fermi-accelerated ions: oxygen ions at MeV energies, protons below ≈300 keV, and alpha particles at intermediate energies. This work concludes by predicting that ion composition and charge state measurements will show the ≈2 MeV events detected by Wind to be due to Fermi acceleration of suprathermal solar wind oxygen ions.

2. Wind Observations

Almost as soon as the three-dimensional plasma and energetic particle (3DP) instrument was turned on, it began to return the first detailed observations of bursts of energetic ions upstream of the bow shock with energies extending to ≈2 MeV [*Sanderson et al.*, 1996; *Skoug et al.*, 1996]. The observations reported by *Skoug et al.* [1996] are shown in Figure 1. The Wind spacecraft was in the solar wind at this time, approaching the bow shock; it crossed the shock at 1920 UT (not shown). Data from the ion solid state telescopes (SSTs) are shown, ranging in energy from 66 keV to 4.44 MeV. The central energy is given for each channel. The fluxes have 6 s time resolution in the low-energy channels and have been averaged over all observed angles. The values shown are in the spacecraft frame of reference.

This period was extremely active and exhibits a number of features familiar from previous observations of upstream energetic ions. A number of bursts reach the ≈1 MeV energy channel, and four bursts, at 1356, 1431, 1639, and 1723 UT, reach the ≈2 MeV energy channel. At a number of times the energy channels below 670 keV show a characteristic plateau-like feature, which has been seen in earlier events [*Lin et al.*, 1974].

IMF data from the Magnetic Fields Investigation (MFI) instrument are also shown in Figure 1. The vertical lines show times of significant IMF rotations that follow each of the first two bursts, at 1404 and 1435 UT, and that coincide with or slightly precede the final two bursts, at 1639 and 1723 UT.

Figure 1 shows that the 1356 and 1431 UT bursts exhibit a dispersion pattern in which the bursts start at lower energies and then appear at higher energies at the end of the burst. This is what is expected of Fermi acceleration, which takes time to develop as particles are reflected between converging barriers. By contrast, the 1639 UT burst appears simultaneously in all energy channels up to the ≈2 MeV channel, and the 1723 UT burst begins simultaneously at all energies and then falls off at the higher energies first while continuing for some time at the lower energies. These bursts could be due to Fermi acceleration that builds up along a field line not connected to the spacecraft, which then moves so that it does connect to the spacecraft when the process has been operating long enough to generate ions of energies up to ≈2 MeV. This would also explain why the 1639 and 1723 UT IMF rotations occur nearly simultaneously with the ion bursts at the spacecraft location.

The November 30, 1994, observations are not unique. There were over 100 ≈2 MeV events observed by Wind from November 1994 to December 1996. The bursts have been observed on both the dawn and dusk sides of the shock and as far upstream as the L1 libration point.

Data from the electron SSTs (not shown) rule out protons and alpha particles for the ≈2 MeV November 30 events and, in general, for ≈2 MeV ions observed on most other days. The protecting foil in front of the electron SSTs will stop protons of energy below 0.4 MeV, alpha particles below 0.85 MeV, and oxygen ions below 3.5 MeV [*Lin et al.*, 1995]. Therefore, if the high-energy counts seen in Figure 1 are due to protons or alpha particles, there should be simultaneous bursts in the electron data. This is not observed, which suggests that the ions responsible for these bursts are probably oxygen, which would not penetrate the foil of the electron detectors. Because the charge state instrument on Wind was not operating yet on November 30, we do not know the charge states of these ions, and it is possible that they could either be solar wind oxygen ions in a high charge state, such as O^{6+}, or magnetospheric ring current particles that have escaped into the solar wind, which would be predominantly O^{+} ions.

There is additional evidence from the Suprathermal and Energetic Particle (STEP) instrument that these bursts consisted of oxygen ions. There were large enhancements (~2 orders of magnitude) in the count rates of CNO group ions; the correspondence between CNO enhancements and the high-energy ion bursts seen with the 3DP SST instrument indicates that the 3DP bursts are probably due to CNO group ions (G. M. Mason, personal communication, 1998). Such enhancements are commonly seen in association with corotating interaction regions (CIRs) in the solar wind [*Mason et al.*, 1996], and although Wind was not in a CIR on November 30, 1994, there had been one the previous day [*Mason et al.*, 1997].

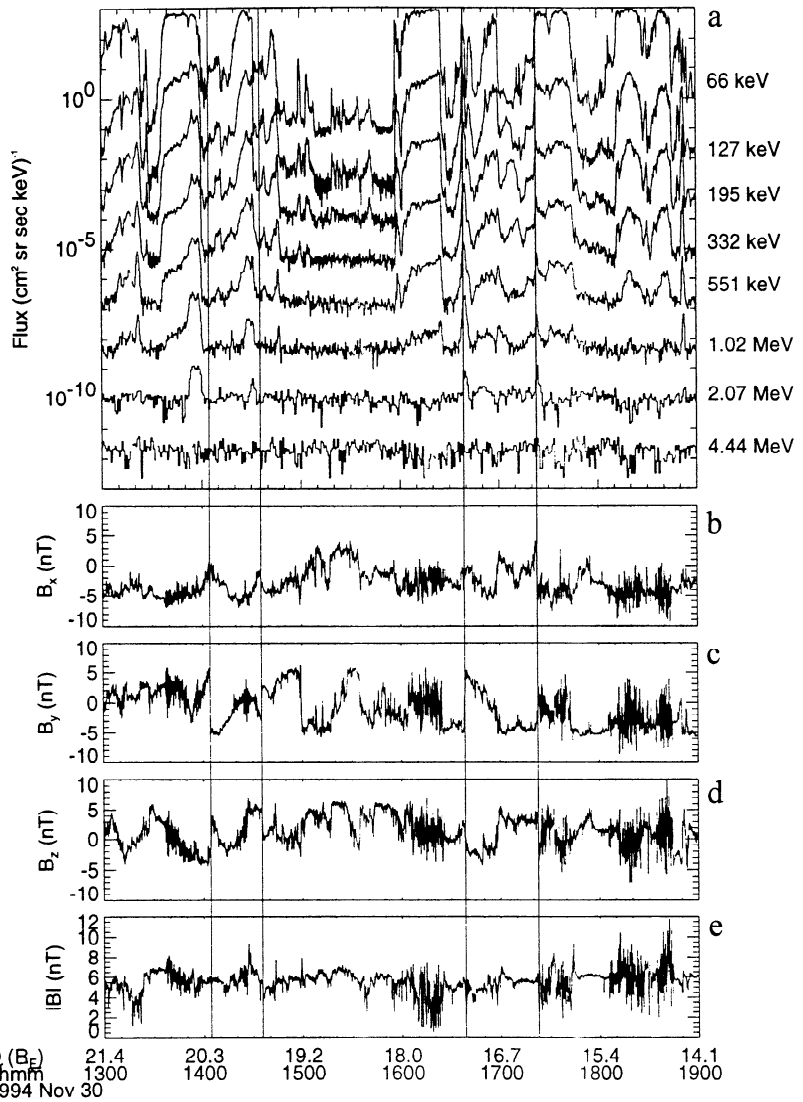

Figure 1. (a) Fluxes from the ion solid state telescopes (SST) on Wind for November 30, 1994. (b)-(e) Each component and the magnitude of the interplanetary magnetic field (IMF). The central energy for each SST channel is given. Fluxes are given in the spacecraft frame of reference and have been averaged over all directions. The flux in the 66 keV channel is the actual value; successive channels have been divided by powers of 10 to separate the data. Vertical lines indicate large IMF rotations that either follow or coincide with the ≈2 MeV ion bursts. The horizontal axis is labeled with the spacecraft distance from the Earth in R_E as well as Universal Time.

3. Fermi Acceleration

First-order Fermi acceleration occurs when two magnetic barriers in space move toward one another; particles initially between them gain energy through repeated reflections. We will consider the problem in the solar wind frame of reference. In that frame the Earth's magnetosphere and bow shock are moving at $-\mathbf{V}_{sw}$ toward the Sun. Particles that are reflected by the bow shock are scattered into the solar wind, where they may be magnetically mirrored or pitch angle-scattered and returned to the shock possibly to be reflected again. With each reflection from the bow shock the particles gain energy in the solar wind frame.

4. De Hoffmann–Teller Reference Frame

In the de Hoffmann–Teller reference frame, there is no electric field, and the shock is stationary [*de Hoffmann and Teller*, 1950]. The transformation between the solar wind frame and the de Hoffmann–Teller frame is shown in Figure 2. Figure 2a shows a monoenergetic segment of an isotropic plasma distribution, represented by a sphere in $v_\perp$–$v_{||}$ space, as well as the angles α and ψ, between the magnetic field direction, and the shock normal and the velocity of the shock ($-\mathbf{V}_{sw}$), respectively. In Figure 2b we transform to the de Hoffmann–Teller frame, first by a transformation of $\mathbf{V}_{sw}$ and then by a velocity $\mathbf{V}_t$ tangential to the shock,

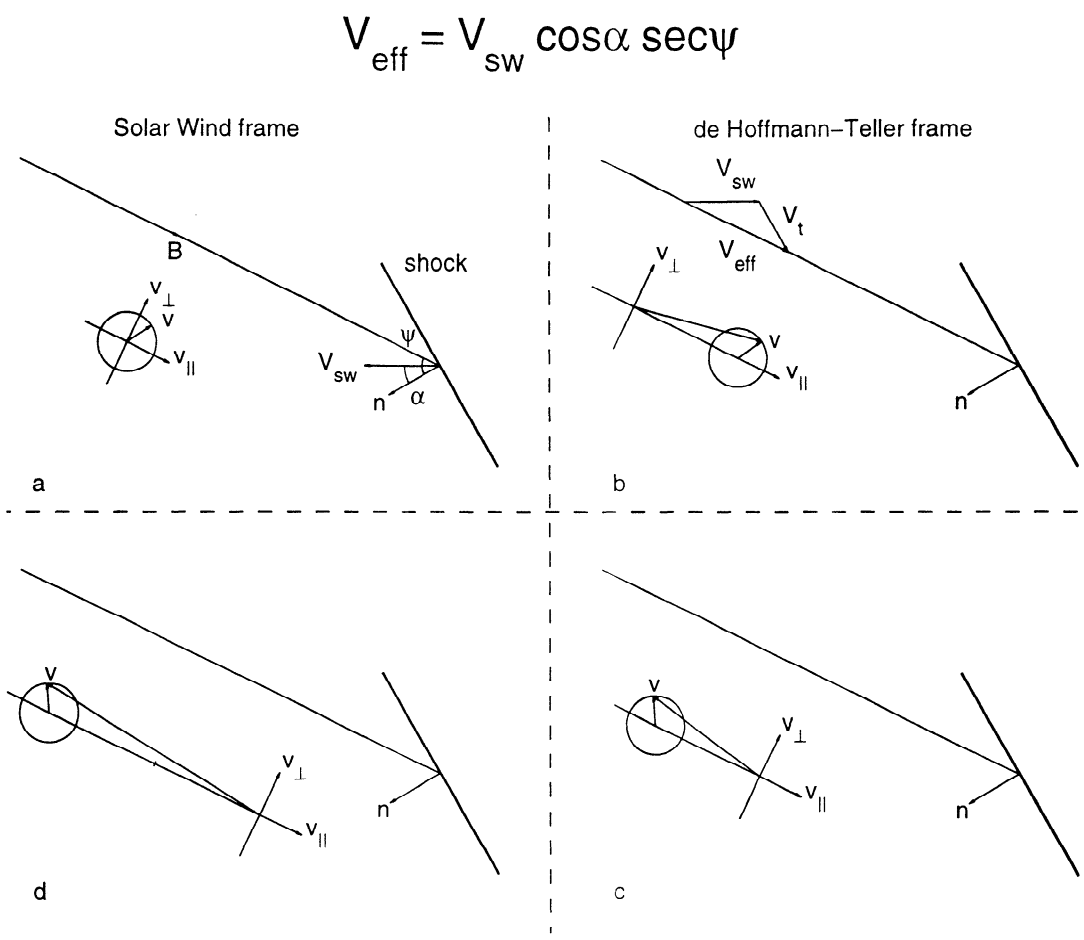

Figure 2. (a) An isotropic distribution in the solar wind frame. (b) The distribution becomes a field-aligned beam in the de Hoffmann–Teller frame. (c) Energy is conserved in the de Hoffmann–Teller frame [*de Hoffmann and Teller*, 1950]. Particles are reflected adiabatically if $v_{||} \rightarrow -v_{||}$. (d) As viewed in the solar wind frame, the particles have gained $-2\mathbf{V}_{eff}$ in velocity.

which maintains the stationarity of the shock. The total transformation velocity between the solar wind and the de Hoffmann–Teller frame, $\mathbf{V}_{eff}$, is parallel to the magnetic field. Since there is no electric field in the solar wind frame and $\mathbf{V}_{eff} \times \mathbf{B} = \mathbf{0}$, there is also no electric field in the de Hoffmann–Teller frame. Similarly, the magnetic field is unchanged by this transformation. The isotropic velocity distribution from the solar wind frame becomes a beam directed along the magnetic field in the de Hoffmann–Teller frame. The transformation velocity is

$$\mathbf{V}_{eff} = \frac{\hat{\mathbf{n}} \cdot \mathbf{V}_{sw}}{\hat{\mathbf{n}} \cdot \hat{\mathbf{b}}} \hat{\mathbf{b}}, \tag{1}$$

where $\hat{\mathbf{b}} = \mathbf{B}/B$ and $\hat{\mathbf{n}}$ is the shock normal. In Figure 2c we consider a reflection mechanism that is adiabatic, in the sense of conserving the first adiabatic invariant. Under such a reflection, $v_{||} \rightarrow -v_{||}$ and $v_\perp \rightarrow v_\perp$. In Figure 2d, we see that in the solar wind frame the particles in this distribution have gained $-2\mathbf{V}_{eff}$ in velocity and become a beam directed back along the magnetic field. As the angle ψ approaches $\pi/2$, the transformation velocity increases well beyond $\mathbf{V}_{sw}$, and thus reflected particles can gain energy very rapidly.

5. Shock Structure

The Earth's bow shock is a fast-mode MHD shock. On the largest scale the shape of the shock is determined by the asymptotic Mach cone angle. On November 30, 1994, the IMF was extremely turbulent, changing direction noticeably on a timescale of minutes. For this reason and because the solar wind flow had high Alfvénic and sonic Mach numbers, the dependence of the Mach cone angle on IMF direction has been ignored. The shock is taken to be a surface of revolution, with the axis of revolution parallel to the solar wind flow direction. Since the IMF was nearly radial, the value of the Mach cone angle is taken to be the maximum value [*Spreiter and Stahara*, 1985],

$$\delta = \arcsin\left(\frac{1}{M_A^2} + \frac{1}{M_S^2}\right)^{1/2}. \tag{2}$$

The overall shape of the shock is taken to be a hyperboloid [*Slavin and Holzer*, 1981; *Slavin et al.*, 1984],

$$r = \frac{L}{1 + \epsilon \cos\theta}, \tag{3}$$

where the eccentricity is determined from the asymp-

totic Mach cone angle $\epsilon = \sec\delta$. The origin of the hyperboloid is determined from the position of the shock at the nose, which was observed by Wind to be 13.6 R_E, and an estimate of the location of the flank of the shock in a direction perpendicular to the Sun-Earth line, which is taken to be 24 R_E [*Elsen*, 1996]. The coordinate axes used throughout this study ("aligned" axes) have been rotated from the GSE axes by $\approx 3°$ in order to align the x_A axis in a direction opposite to the flow velocity of the solar wind. These coordinates are useful because the plasma flow direction determines the orientation of the bow shock. For most purposes one can consider the x_A–y_A plane to be the equatorial plane and the x_A–z_A plane to be the plane of the noon-midnight meridian.

Locally, the upstream plasma parameters and the shock geometry uniquely determine the downstream plasma parameters, through the Rankine-Hugoniot conditions [e.g., *Petrinec and Russell*, 1997]. Average measured solar wind properties for the 6 hour period 1300–1900 UT, November 30, 1994, were solar wind velocity of 542 km s^{-1}, plasma thermal temperature of 23.8 eV, ion density of 4.2 cm^{-3}, plasma beta of 1.4, Alfvénic Mach number of 9.5, and sonic Mach number of 8.8.

6. Shock Drift Acceleration

Ions are reflected by the shock and gain energy in the solar wind frame of reference in a process known as shock drift acceleration [e.g., *Armstrong et al.*, 1985]. In the case of particle reflection from the Earth's bow shock the first adiabatic invariant is nearly conserved for quasi-perpendicular shocks, while for quasi-parallel shocks, there is a spread in the pitch angle distribution that is roughly centered on the adiabatic solution [*Freeman*, 1998]. Thus the discussion of Figure 2 can be usefully employed in describing the energy gained by particles that are reflected from the shock. Reflected particles conserve energy in the de Hoffmann–Teller frame and therefore gain energy in the solar wind frame, where there is an electric field $\mathbf{E} = \mathbf{V}_{eff} \times \mathbf{B}$ downstream of the shock, and a resulting $\mathbf{E} \times \mathbf{B}$ drift motion.

The model presented in this study relies upon the fact that a single field line can be connected to the shock in a quasi-perpendicular configuration at one time and within a few minutes change to a quasi-parallel configuration, or vice versa, simply because of an IMF rotation. A suprathermal oxygen ion that is first reflected at the quasi-parallel shock can gain a factor of $\approx$2–6 in energy; if it is pitch angle-scattered upstream and returns to the shock at a location where the geometry is quasi-perpendicular, it can then increase its energy by a factor of $\approx$10 [*Freeman*, 1998]. This is in contrast to previous models of Fermi acceleration, which generally modeled particle motion in one or two dimensions, using either a quasi-parallel or quasi-perpendicular geometry but not both [e.g., *Terasawa*, 1979; *Lee et al.*, 1982; *Ellison*, 1985; *Decker and Vlahos*, 1986];

7. Particle Reflection From IMF Rotations

The IMF went through a number of large rotations on November 30, 1994. We now model the effect of large-scale IMF rotations on particle motion by following particle trajectories in a simplified field. In this calculation one component of magnetic field, B_z, rotates uniformly from 4 to −4 nT over a distance of $2R_E$, which is approximately the distance the solar wind moved past the spacecraft during the 1404 UT rotation. Another component, B_x, remains a constant 4 nT. The magnitude of the field goes through a minimum during the rotation. As a result, low-energy particles that conserve the first adiabatic invariant will simply traverse the region of the rotation. However, the motion of suprathermal ions must be treated with a full calculation of the Lorentz force motion.

In Figure 3, projections of particle orbits are shown. Figure 3a shows several examples of numerically computed orbits of O^{6+} ions in this model rotation. Low-energy particles, such as a 1 keV O^{6+} ion, behave nearly adiabatically. As particle energy increases, the behavior becomes nonadiabatic, and as the particle gyroradius becomes comparable to the transition width, the particles are often reflected by the rotation, as with the 100 keV O^{6+} ion shown. This process is very similar to particle reflection from the shock, as viewed in the de Hoffmann–Teller reference frame.

Figure 3b shows the fraction of particles, sampled from an isotropic distribution, that are reflected by the rotation. For each energy shown, 100,000 particle orbits have been computed. We see that the rotation reflects 10–25% of the suprathermal ions (10–100 keV) and that reflection efficiency is generally an increasing function of energy over the energy range 1 keV to 1 MeV.

This reflection of suprathermal ions by IMF rotations, in conjunction with shock drift acceleration, establishes the physics of Fermi acceleration at the Earth's bow shock. Suprathermal ions that are reflected between these approaching structures gain energy.

8. Interplanetary Magnetic Field

A satellite can only measure the IMF at a single point, so in order to use IMF data to estimate the field at other locations we must make an assumption about the nature of the field. In this study we assume that the field is a static plane wave in the solar wind frame, translationally invariant in all directions perpendicular to some chosen direction. To maintain a divergenceless field, the component of the field in this chosen direction is set to a constant value. This assumption modifies the field, clearly leading to some inaccuracy, but it also allows us to extend the observed field to fill a three-dimensional volume of space, allowing the calculation of particle trajectories. In order to minimize the modification of the field the direction in which the field is set to a constant value is chosen to be the mean field

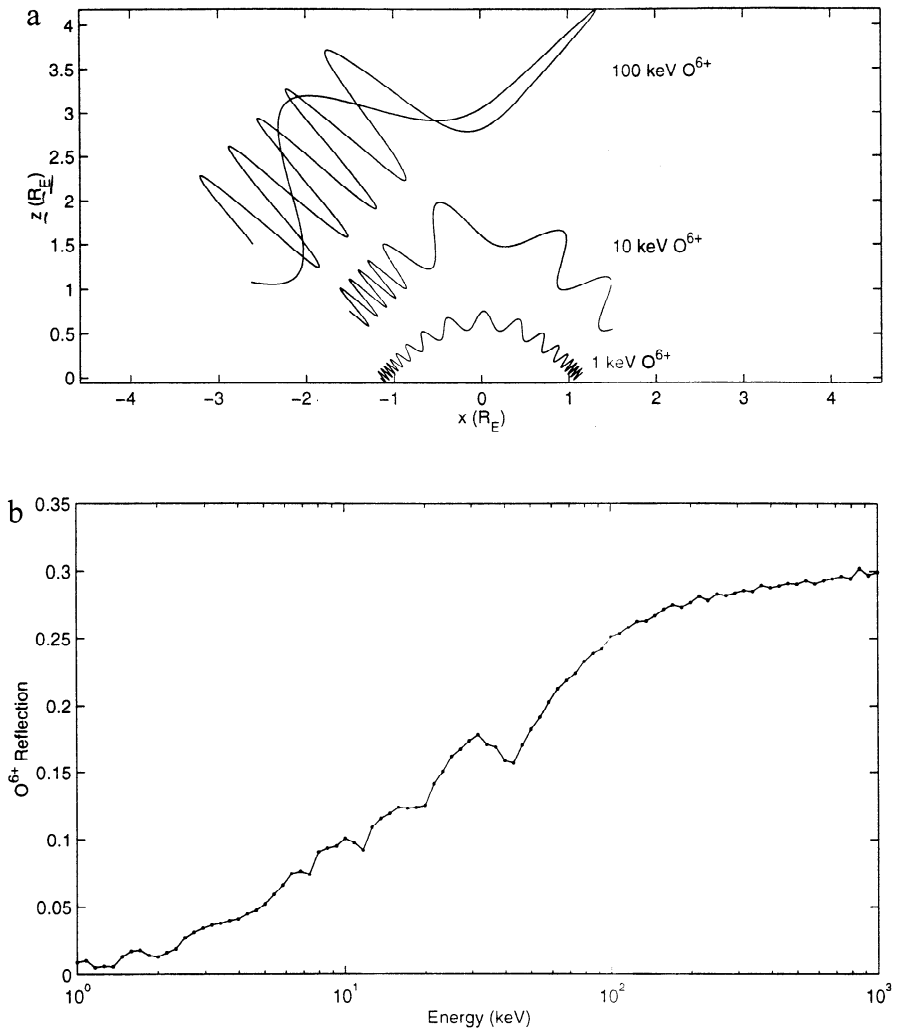

Figure 3. (a) Projections of particle orbits in a simplified model of the 1404 UT rotation. In this model, B_z rotates from 4 to -4 nT from $x = -1R_E$ to $x = 1R_E$ while remaining constant outside of this transition region. The B_x component is a constant 4 nT. The 1 and 10 keV O^{6+} ions shown traverse the transition region, while the 100 keV ion is reflected. (b) The probability of reflection, as a function of energy, for particles drawn from an isotropic distribution.

direction over the interval 1300–1900 UT. A minimum variance analysis of the IMF yields the direction normal to local planes of magnetic discontinuity. For this entire 6 hour interval the normal direction determined by minimum variance is $<22°$ from the mean field direction. Since the field is primarily radial at this time, the GSE component most altered is the x_{GSE} component.

By using MFI data for the magnetic field, with a time resolution of 3 s, and assuming that the IMF is a static plane wave in the solar wind frame, we have ignored the effect of wave turbulence on particle motion. Our intention is to demonstrate that bursts of upstream ions in the MeV energy range can be explained by Fermi acceleration due to multiple reflections between IMF rotations and the bow shock. Wave turbulence is not a necessary feature of the model, although including it could help explain the origin of the seed population of upstream diffuse ions.

9. Single Particle Motion

Figure 4 shows projections into the x_A–y_A and x_A–z_A planes of an O^{6+} ion trajectory. This particle starts at the bow shock with an energy of 68 keV at 1400 UT, just before the large IMF rotation associated with the first $\approx$2 MeV burst reaches the spacecraft. It is accelerated through multiple bow shock crossings, reaching 1.38 MeV in <9 min. The projection of several IMF lines at 1403:47 UT, when the particle is turned around in the solar wind, is also shown. The energy shown in Figure 4c is the particle energy as viewed in the solar wind frame. Each time the particle crosses the shock, the Rankine-Hugoniot relations are solved to find the electric and magnetic fields downstream. The particle experiences an $\mathbf{E} \times \mathbf{B}$ drift while downstream. The resulting sinusoidal variation in kinetic energy with time is phased such that when the particle recrosses the

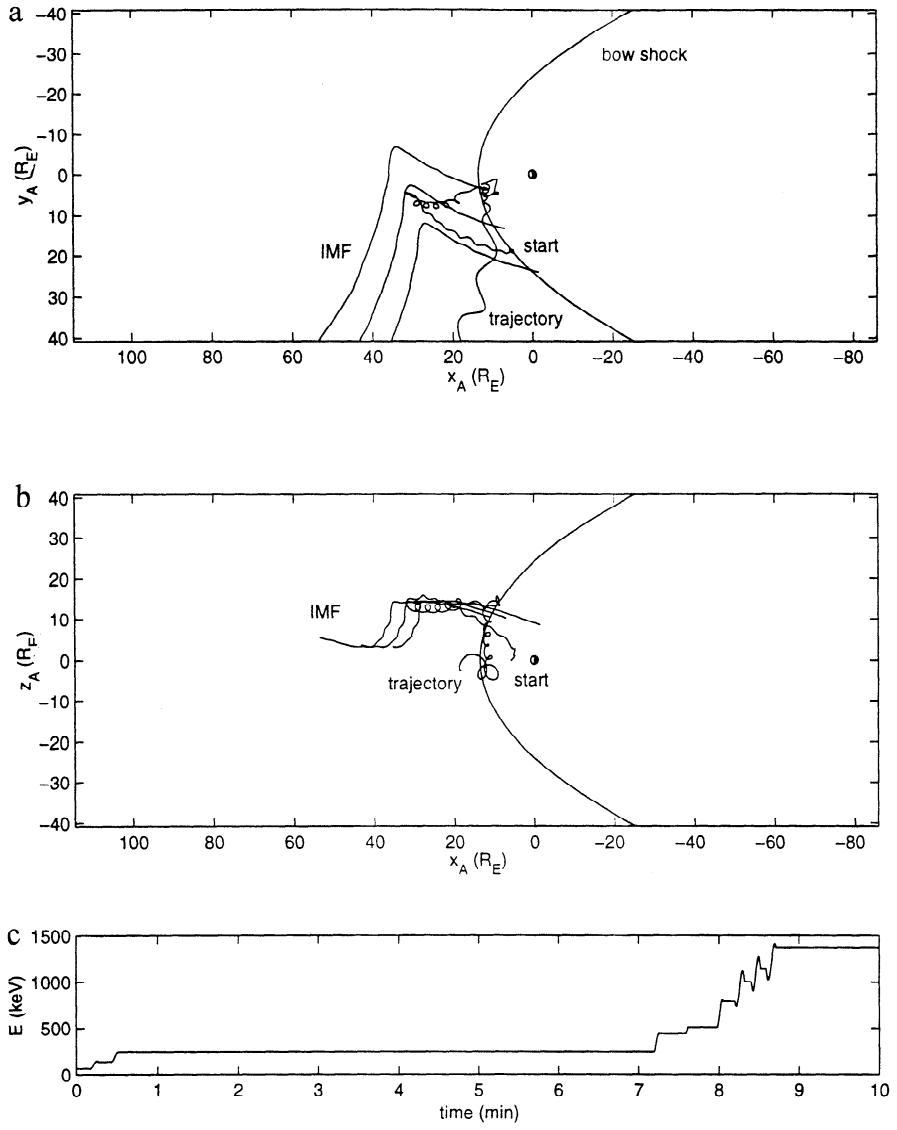

Figure 4. (a) and (b) Projections of the motion of a suprathermal O^{6+} ion into the x_A-y_A and x_A-z_A planes, where the x_A axis is aligned in the $-\mathbf{V}_{sw}$ direction. The ion starts at the shock ($x_A = 5.9\ R_E$, $y_A = 18.4\ R_E$, and $z_A = 0\ R_E$) with an energy of 68 keV and reaches an energy of 1.38 MeV in <9 min. The first two shock crossings occur at the start of the particle's motion, when the gyroradius is small. The projection of several IMF lines is shown at 1403:47 UT, when the particle is turned around in the solar wind. (c) The particle's kinetic energy in the solar wind frame.

shock, it has gained energy in the solar wind frame of reference. This is equivalent to noting that energy is a constant of the motion in the de Hoffmann–Teller frame and, as a result, increases in the solar wind frame because of reflection from a moving magnetic barrier.

10. Simulated Wind Observations

We now approach the problem statistically, starting a large number of ions uniformly across the entire area of the shock forward of $x_A = 0$, with starting times uniformly distributed over a specified time interval. Particles are emitted isotropically from the shock at all angles from 0 to $\pi/2$ with respect to the local shock normal direction. Particle energies are drawn from the suprathermal distribution (upstream diffuse ions), in the 20-100 keV energy range, using the differential flux observed by *Lin et al.* [1974], $dJ/dE \sim E^{-3}$.

In simulating Wind data, only those particles that reach the location of the spacecraft are counted. In order to detect a reasonable number of particles the "spacecraft location" is taken to be a sphere of radius 1 R_E, centered on the spacecraft location. Particles that reach a free escape boundary, defined as $x_A = \pm 60 R_E$, or a cylindrical distance $\sqrt{y_A^2 + z_A^2} = 50 R_E$, are not followed further.

Results of this simulation are shown in Figure 5 for the time interval 1330–1500 UT. In this simulation, 500 million O^{6+}, 100 million He^{2+}, and 40 million H^+ ion trajectories were followed. Figure 5 shows the particle

energy plotted with time. There is good correspondence between the simulated data and the Wind observations of Figure 1. The simulation has bursts that extend to the ≈2 MeV channel at 1356 and 1428 UT, corresponding closely with the timing of the observed bursts. The interval 1427:45-1428:15 UT is indicated by vertical lines. This interval is used in Figures 6 and 8 to compare the simulation with the burst observed at 1431 UT. (The simulated data occur slightly earlier than the observations because of an approximation used in the simulation. In order to facilitate the computation of field lines the satellite motion was taken to be linear. As a result, the IMF convects more rapidly in this interval than it really did on November 30.) The timescale of the simulated bursts is of the order of several minutes, which agrees with the observations. Both of these bursts appear in the low-energy channels first and then reach the high-energy channels briefly, which is also seen in the observations. The count rates in the low-energy channels exhibit the same plateau-like features observed by Wind. Bursts at 1410 and 1445 UT, which extend to the ≈1 MeV channel, also resemble bursts observed at those times by Wind. The energy per charge of the peaks in each simulated data set is quite similar. The maximum E/q ratios for H^+, He^{2+}, and O^{6+} during this interval are 333, 300, and 332 keV/q, respectively. Thus we have extended to these higher energies the result that Fermi acceleration produces E/q ratios that are roughly independent of species, without assuming a diffusion coefficient that is a function of energy per charge, as has been postulated in previous models [*Lee et al.*, 1981; *Forman*, 1981; *Ellison*, 1981].

One difference between the simulation and the data is that the data show a sudden drop in all channels at the end of the 1356 UT burst, while the simulation shows continuing activity in the low-energy channels. This is probably because of differences between the plane wave magnetic field approximation used in the simulation and the real IMF. The correspondence is better for the 1431 UT burst, and in fact, the plane wave magnetic field used in the simulation agrees with the IMF data better at that time [*Freeman*, 1998]. Since this process is controlled by the geometry of the IMF and the bow shock, it is no surprise that the fidelity of the model used for magnetic field to the data is a predictor of accuracy in the simulation.

11. Simulated and Observed Particle Distributions

Figure 6 shows a comparison between the ion flux from the Wind SST detectors during the large ≈2 MeV burst at 1431:05-1431:36 UT and the corresponding simulated burst, which peaks during the interval indicated in Figure 5, 1427:45-1428:15 UT. In Figure 6a the SST data are fit to a power law spectrum $E^{-\gamma}$, with $\gamma = 4.16$. In Figure 6b a fit of the simulated spectra for H^+, He^{2+}, and O^{6+} to the observed spectrum is shown.

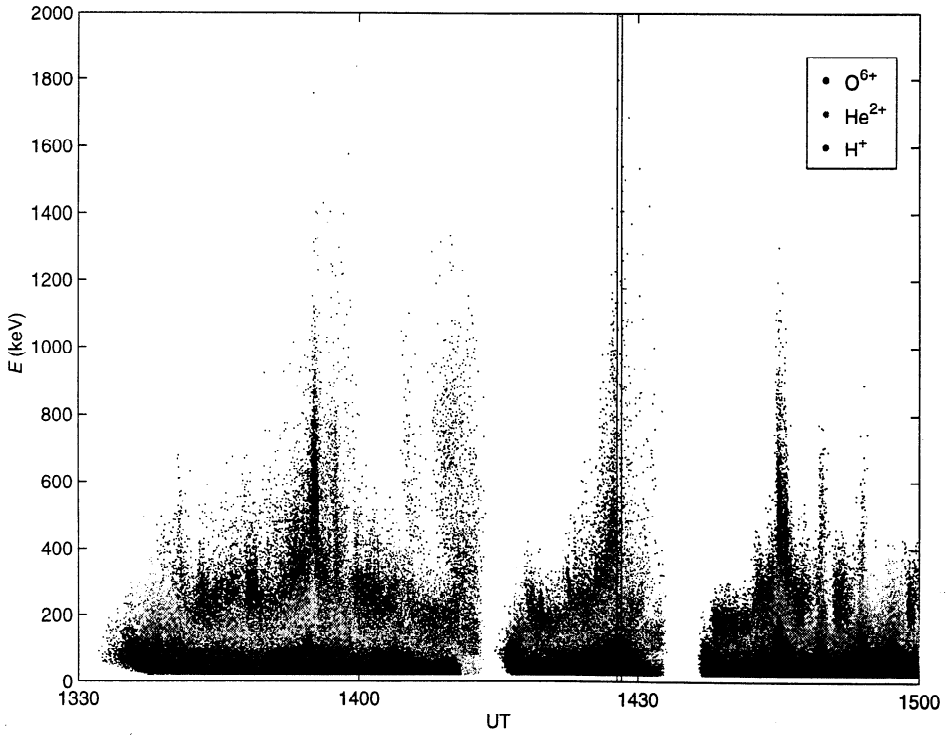

Figure 5. Simulated observations at the spacecraft location of H^+, He^{2+}, and O^{6+} ions are shown together. The interval 1427:45-1428:15 UT (indicated by vertical lines) is used to calculate the simulated fluxes shown in Figure 6.

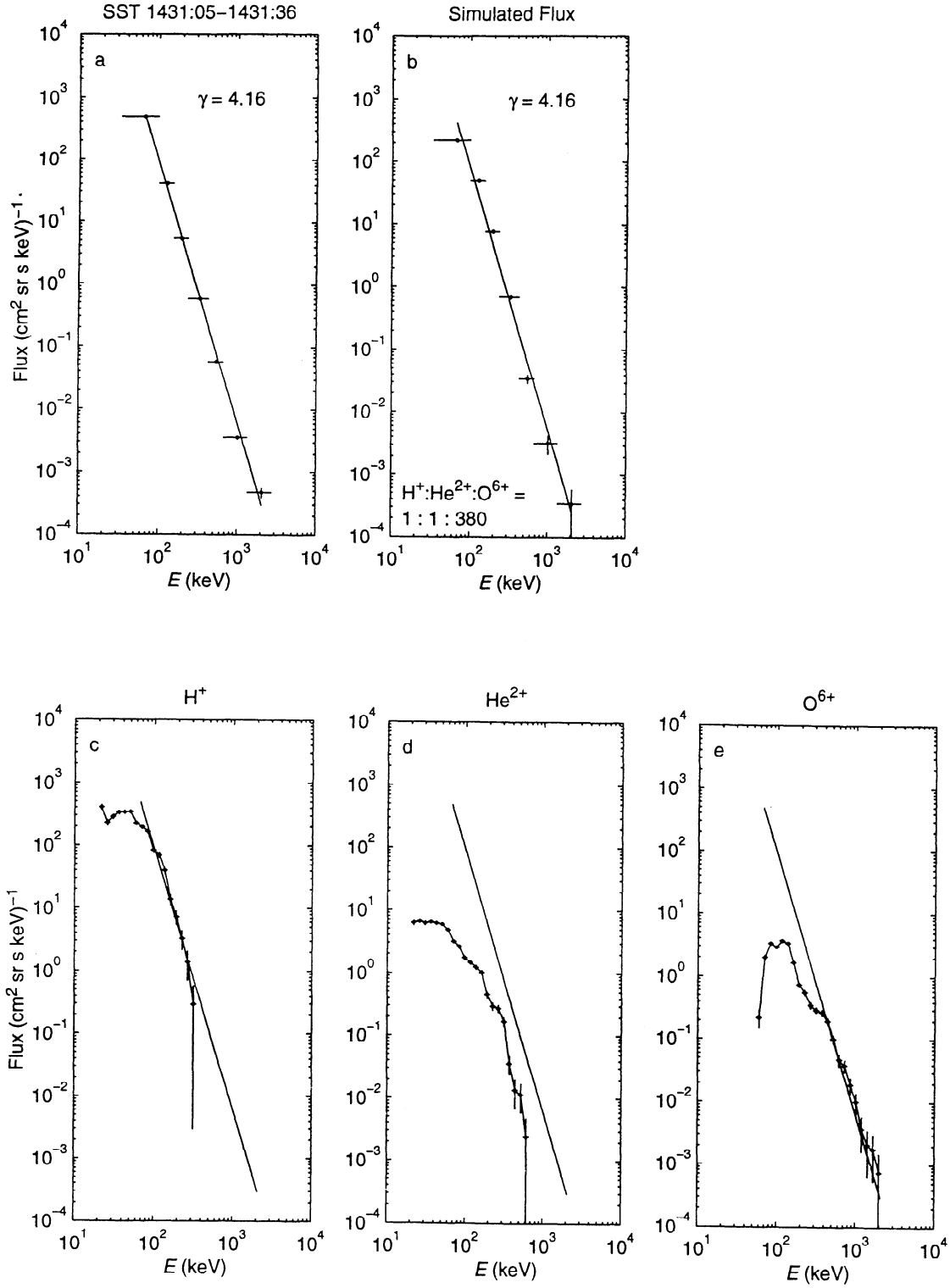

Figure 6. (a) Flux measured during the second ≈2 MeV burst for the interval 1431:05-1431:36 UT. (b) Simulated spectra of H^+, He^{2+}, and O^{6+} ions are added together in the ratio of 1:1:380 relative to solar wind abundances to fit the data. Note that the peak of the simulated burst occurs for the interval shown in Figure 5, 1427:45-1428:15 UT, because of approximating the spacecraft motion as linear. (c)-(e) Individual simulated spectra for each species with the O^{6+} flux again enhanced by a factor of 380. The observed power law spectrum from Figure 6a is also shown. The energy bins used in Figures 6c-6e are much narrower than the actual SST bins, which are used in Figures 6a and 6b. Also, the energy loss of ions in the dead layer of the instrument is not taken into account in Figures 6c-6e, while it is in Figure 6b.

Simulated counts for each species are sorted separately according to the mass-dependent values of the boundaries between energy bins; for example, the ≈2 MeV channel detects protons in the range 1.36-2.79 MeV and oxygen ions in the range 1.78–3.35 MeV. In order to fit the observed spectrum the abundance of oxygen was increased by a factor of 380 relative to solar wind abundance, while the abundance of protons and alpha particles was unchanged. Average solar wind abundances of 0.04 for helium and 5.2×10^{-4} for oxygen were used [*Galvin et al.*, 1984]. Figures 6c–6e show the simulated fluxes for each species separately, with the O^{6+} spectrum again enhanced by a factor of 380. The energy bins used in these plots are much narrower than the actual bins used by Wind, and the loss of energy in the dead layer of the detectors is ignored. The power law fit from Figure 6a is shown for comparison. The proton and oxygen spectra match the observations quite well at the low and high ends, respectively. The helium spectrum matches the observed slope well for intermediate energies but is lower in magnitude than the observed flux. Comparisons between observation and simulation yield a similar result at other times during this 90 min interval. It must be emphasized that this fit does not require an overall enhancement of the abundance of solar wind oxygen; it only requires a large enhancement of the amount of solar wind oxygen in the suprathermal energy range, above 20 keV. Enhancements of CNO group elements above 40 keV/q, measured by STEP, were of this order of magnitude during this interval.

The enhancement of 380 in the the seed population of suprathermal solar wind oxygen ions calculated in the fit shown in Figure 6 is much higher than the average enhancement of 1.6 in helium at ~30 keV/q during diffuse upstream ion events reported by *Ipavich et al.* [1984]. However, the actual enhancement of the seed O^{6+} ions need not be so extreme if it occurs over a small region of the shock or with different spectral characteristics than

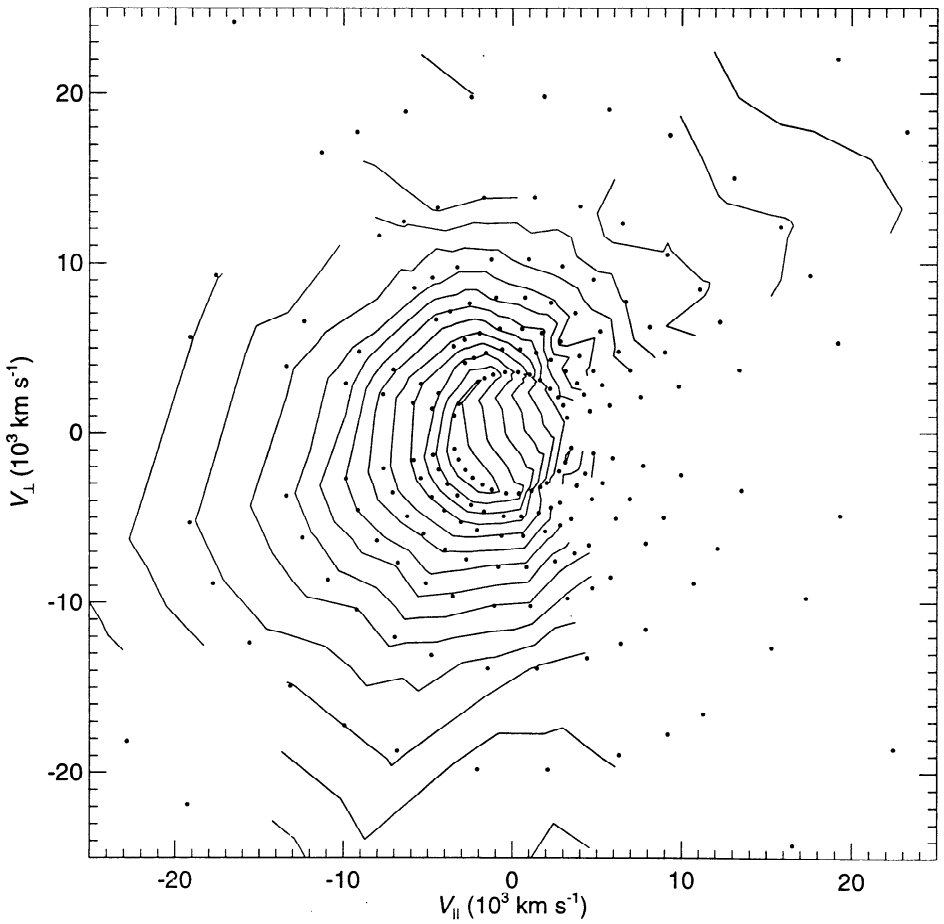

Figure 7. The observed distribution function is shown for the interval 1431:05-1431:36 UT. The three-dimensional distribution has been folded into the the plane defined by the solar wind velocity and the magnetic field, with some gyrotropic features retained in the sign of $v_\perp$. The detector does not differentiate ion species, so all ions are assumed to be protons. Contours of constant distribution function are plotted on a logarithmic scale. The solid points indicate the location of the pitch angle bins; features smaller than the spacing between bins are not physically meaningful. The distribution shows that the burst is primarily directed upstream, away from the shock (in the negative $v_{||}$ direction).

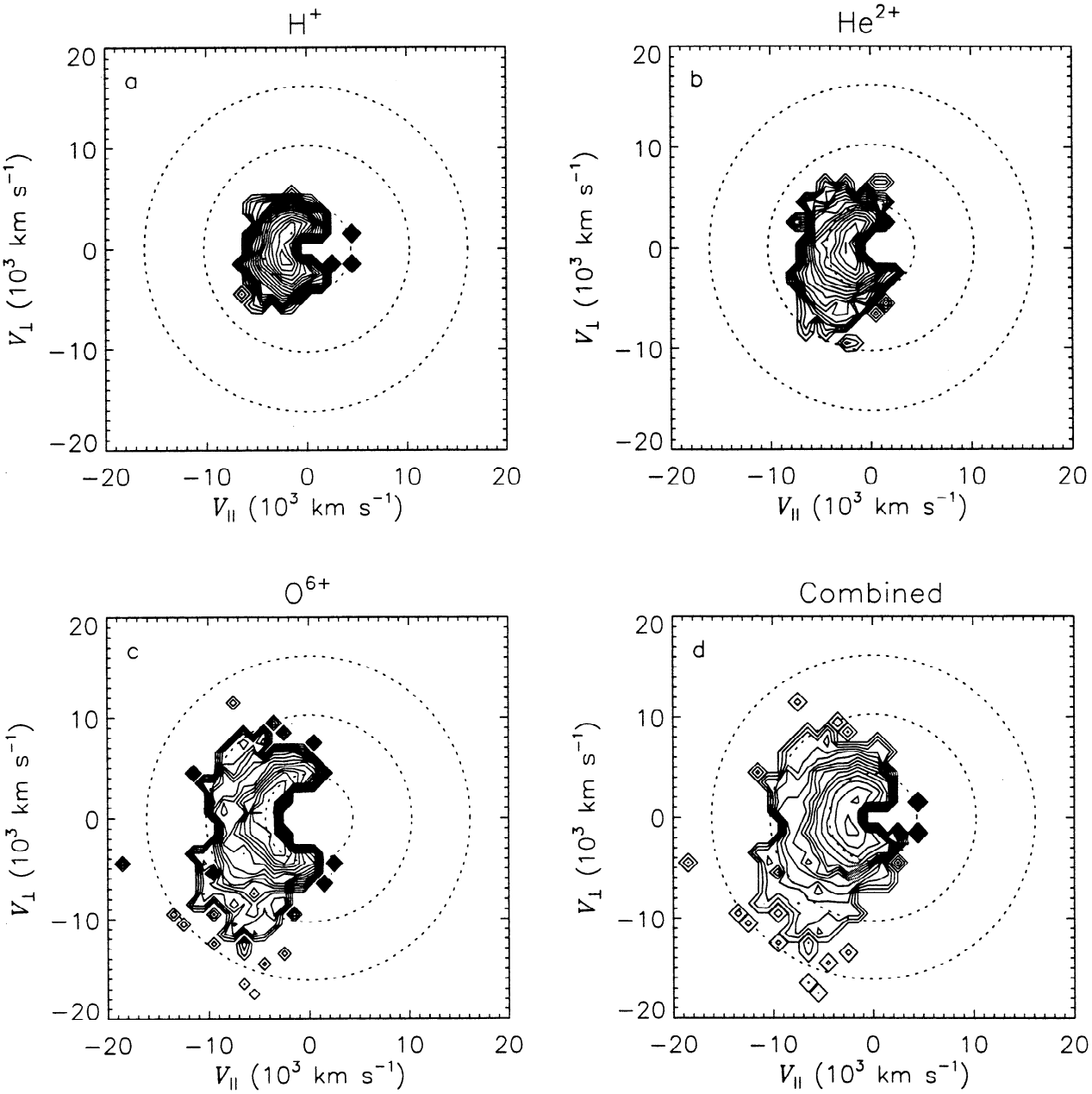

Figure 8. The simulated H^+, He^{2+}, and O^{6+} distribution functions for the interval 1427:45-1428:15 UT are shown separately and combined in Figure 8d, again using the ratio of 1:1:380 relative to solar wind abundances. Particle velocities have been calculated under the assumption that the particles are protons. The dashed circles correspond to proton energies of 100, 550, and 1360 keV. (The minimum energy for a proton to be counted in the ≈2 MeV channel is 1360 keV.) The combined distribution function shows a similar upstream flow to the observed distribution function shown in Figure 7 and even exhibits a similar nongyrotropic preference for the negative $v_\perp$ direction.

the proton spectrum. We do not suggest that this value of 380 is predictive as it depends on the assumed input distribution; we only suggest that some enhancement in the seed population of suprathermal solar wind oxygen ions is necessary.

Figure 7 shows the distribution function from the ion SSTs for the same interval as is shown in Figure 6, 1431:05-1431:36 UT. Here the three-dimensional distribution has been folded into the plane defined by the solar wind flow velocity and the magnetic field. Since the 3DP instrument cannot distinguish different ion species, Figure 7 was constructed under the assumption that all detected ions are protons. Particles have been sorted into the upper (lower) half plane of Figure 7 if the sign of $\mathbf{v} \cdot (\mathbf{V}_{sw} \times \mathbf{B})$ is positive (negative), where $\mathbf{v}$ is the particle velocity. Solid dots indicate the locations of angle bins for this interval. Structures that have a scale size smaller than the bin spacing are not physically mean-

ingful. The distribution function is anisotropic, with many more particles streaming away from the Earth's bow shock (in the negative $v_{||}$ direction) than toward the shock. This is especially true for energies above 2 MeV (velocities above 2×10^4 km s^{-1}).

In Figure 8 the simulated data have been treated in the same fashion. Each species is plotted separately, and the three are added together in Figure 8d, again using the abundance ratio of 1:1:380 relative to average solar wind abundances. In order to facilitate a comparison with the data shown in Figure 7, particle energies are used to calculate velocity, assuming the ions are protons. Dashed circles indicate velocities of protons of 100, 550, and 1360 keV. Protons need a minimum energy of 1360 keV to be counted in the ≈2 MeV energy channel. The resulting simulated distribution function looks remarkably similar to that of Figure 7. The simulation suggests that the Wind data consisted primarily of protons below ≈100 keV, with Fermi-accelerated solar wind oxygen ions making up the high-energy component of the distribution.

12. Discussion and Conclusions

The physics of the Fermi acceleration process presented here lies in the magnetic field geometry of the IMF and the bow shock. The discontinuity of the tangential component of the magnetic field at the shock reflects ions in a process that is nearly adiabatic, on average. Suprathermal O^{6+} ions are reflected efficiently from the quasi-parallel shock, where they gain enough energy to be subsequently reflected at the quasi-perpendicular shock. After 5–10 reflections at the quasi-perpendicular shock, O^{6+} ions can reach MeV energies. On the other hand, protons and alpha particles only reach several hundred keV through this process. By using measured IMF data and a realistic shock geometry the model presented here incorporates both quasi-perpendicular and quasi-parallel shocks.

The IMF also provides the second reflector necessary for Fermi acceleration. Energetic ions with a gyroradius that is comparable to the scale length of an IMF rotation can be reflected by the rotation in a manner similar to shock reflection. Because of this, the bursts of ≈2 MeV particles coincide with IMF rotations, both in the observations and in the model.

The Fermi process requires more than just two reflectors moving toward one another, however. It also requires that the particles remain between the reflectors long enough to reach the energies one is attempting to explain. This has been demonstrated in this study by the calculation of single-particle trajectories. Counting particles only when they reach the spacecraft location, it is found that the resulting fluxes closely resemble the Wind observations if the high-energy tail of the solar wind oxygen distribution is enhanced by ~2 orders of magnitude. In association with these bursts the STEP experiment did measure elevated fluxes of CNO ions on November 30, 1994.

Interplanetary magnetic field data will also provide an important test of the Fermi model presented here. A careful study of the geometry of the IMF in relation to the position of the spacecraft and the location of the shock is needed to differentiate between those events that are similar to the November 30 events, in that the spacecraft was in position to observe both the ≈2 MeV ion fluxes and the coincident IMF rotations, and those that are not. It is possible for IMF rotations to cause Fermi acceleration of ions that reach the spacecraft without the rotations themselves being observed. In such cases it may be possible to test the Fermi model by using IMF data from more than one spacecraft. The crucial test of this model, however, that is necessary to settle the issue of whether upstream MeV ion events are due to Fermi acceleration of solar wind ions, rather than leakage of high energy ions from the magnetosphere, will come from charge state and ion composition measurements of these bursts.

In this study we have used observations from the Wind spacecraft and the numerical calculation of over 600 million individual ion trajectories to make a prediction. We predict that upstream ions in the MeV energy range are suprathermal solar wind O^{6+} ions that have undergone Fermi acceleration through multiple reflections between the shock and IMF rotations.

Acknowledgments. We thank G. M. Mason for the STEP/EPACT data used in this study. We also thank R. M. Winglee for useful discussions. The Wind project is supported by NASA grants NAG5-26580 at the University of Washington and NAG5-2815 at the University of California, Berkeley.

Hiroshi Matsumoto thanks M. Scholer and T. Terasawa for their assistance in evaluating this paper.

References

Anagnostopoulos, G. C., E. T. Sarris, and S. M. Krimigis, Magnetospheric origin of energetic (E ≥ 50 keV) ions upstream of the bow shock: The October 31, 1977, event, *J. Geophys. Res., 91*, 3020-3028, 1986.

Anderson, K. A., Measurements of bow shock particles far upstream from the Earth, *J. Geophys. Res., 86*, 4445-4454, 1981.

Armstrong, T. P., M. E. Pesses, and R. B. Decker, Shock drift acceleration, in *Collisionless Shocks in the Heliosphere: Reviews of Current Research, Geophys. Monogr. Ser.*, vol. 35, edited by B. T. Tsurutani and R. G. Stone, pp. 271-285, AGU, Washington, D. C., 1985.

Asbridge, J. R., S. J. Bame, and I. B. Strong, Outward flow of protons from the Earth's bow shock, *J. Geophys. Res., 73*, 5777-5782, 1968.

Ashford, S. M., The origin of the suprathermal seed population for the Fermi acceleration of ions at the Earth's bow shock, Ph.D. thesis, Univ. of Calif., Berkeley, 1998.

Baker, D. N., R. D. Belian, T. A. Fritz, P. R. Higbie, S. M. Krimigis, D. G. Sibeck, and R. D. Zwickl, Simultaneous energetic particle observations at geostationary orbit and in the upstream solar wind: Evidence for leakage during the magnetospheric compression event of November 1, 1984, *J. Geophys. Res., 93*, 14,317-14,327, 1988.

Decker, R. B., and L. Vlahos, Numerical studies of particle acceleration at turbulent, oblique shocks with an ap-

plication to prompt ion acceleration during solar flares, *Astrophys. J., 306*, 710-729, 1986.

de Hoffmann, F., and E. Teller, Magneto-hydrodynamic shocks, *Phys. Rev., 80*, 692-703, 1950.

Eichler, D., Energetic particle spectra in finite shocks: The Earth's bow shock, *Astrophys. J., 244*, 711-716, 1981.

Ellison, D. C., Monte Carlo simulation of charged particles upstream of the Earth's bow shock, *Geophys. Res. Lett., 8*, 991-994, 1981.

Ellison, D. C., Shock acceleration of diffuse ions at the Earth's bow shock: Acceleration efficiency and A/Z enhancement, *J. Geophys. Res., 90*, 29-38, 1985.

Elsen, R. K., Global modeling of the average response of the magnetosphere to varying solar wind conditions, Ph.D. thesis, Univ. of Wash., Seattle, 1996.

Forman, M. A., First-order Fermi acceleration of the diffuse ion population near the Earth's bow shock, paper presented at *17 International Conference on Cosmic Rays*, Cosmic Ray Commission of the International Union of Pure and Applied Physics, Paris, *3*, 467-470, 1981.

Freeman, T. J., A study of Fermi acceleration of suprathermal solar wind ions, Ph.D. thesis, Univ. of Wash., Seattle, 1998.

Galvin, A. B., F M. Ipavich, G. Gloeckler, D. Hovestadt, B. Klecker, and M. Scholer, Solar wind temperatures inferred from the charge state composition of diffuse particle events, *J. Geophys. Res., 89*, 2655-2671, 1984.

Ipavich, F. M., J. T. Gosling, and M. Scholer, Correlation between the He/H ratios in upstream particle events and in the solar wind, *J. Geophys. Res., 89*, 1501-1507, 1984.

Kudela, K., D. G. Sibeck, R. D. Belian, S. Fischer, and V. Lutsenko, Possible leakage of energetic particles from the magnetosphere into the upstream region on June 7, 1985, *J. Geophys. Res., 95*, 20,825-20,832, 1990.

Lee, M. A., Coupled hydromagnetic wave excitation and ion acceleration upstream of the Earth's bow shock, *J. Geophys. Res., 87*, 5063-5080, 1982.

Lee, M. A., G. Skadron, and L. A. Fisk, Acceleration of energetic ions at the Earth's bow shock, *Geophys. Res. Lett., 8*, 401-404, 1981.

Lin, R. P., C.-I. Meng, and K. A. Anderson, 30 to 100 keV protons upstream from the Earth's bow shock, *J. Geophys. Res., 79*, 489-498, 1974.

Lin, R. P., et al., A three-dimensional plasma and energetic particle investigation for the Wind spacecraft, *Space Sci. Rev., 71*, 125-153, 1995.

Mason, G. M., J. E. Mazur, and T. T. von Rosenvinge, Energetic heavy ions observed upstream of the Earth's bow shock by the STEP/EPACT instrument on Wind, *Geophys. Res. Lett., 23*, 1231-1234, 1996.

Mason, G. M., J. E. Mazur, J. R. Dwyer, D. V. Reames, and T. T. von Rosenvinge, New spectral and abundance features of interplanetary heavy ions in corotating interaction regions, *Astrophys. J., 486*, L149-L152, 1997

Möbius, E., D. Hovestadt, B. Klecker, M. Scholer, F. M. Ipavich, C. W. Carlson, and R. P. Lin, A burst of energetic O^+ ions during an upstream particle event, *Geophys. Res. Lett., 13*, 1372-1375, 1986.

Petrinec, S. M., and C. T. Russell, Hydrodynamic and MHD equations across the bow shock and along the surfaces of planetary obstacles, *Space Sci. Rev., 79*, 757-791, 1997.

Sanderson, et al., Wind observations of energetic ions far upstream of the Earth's bow-shock, *Geophys. Res. Lett., 23*, 1215-1218, 1996.

Sarris, E. T., G. C. Anagnostopoulos, and S. M. Krimigis, Simultaneous measurements of energetic ion ($\geq$50 keV) and electron ($\geq$220 keV) activity upstream of Earth's bow shock and inside the plasma sheet: Magnetospheric source for the November 3 and December 3, 1977, upstream events, *J. Geophys. Res., 92*, 12,083-12,096, 1987.

Scholer, M., D. Hovestadt, F. M. Ipavich, and G. Gloeckler, Upstream energetic ions and electrons: Bow shock-associated or magnetospheric origin?, *J. Geophys. Res., 86*, 9040-9046, 1981.

Scholer, M., E. Möbius, L. M. Kistler, and F. M. Ipavich, Correlated observations of energetic particles upstream of the bow shock, in the magnetosheath, and in the magnetosphere, *J. Geophys. Res., 95*, 21,297-21,305, 1990.

Scholer, M., H. Kucharek, and K. J. Trattner, Injection and acceleration of energetic particles at collisionless shocks, *Adv. Space Res., 21*, 4, 533-542, 1998.

Sibeck, D. G., R. W. McEntire, S. M. Krimigis, and D. N. Baker, The magnetosphere as a sufficient source for upstream ions on November 1, 1984, *J. Geophys. Res., 93*, 14,328-14,342, 1988.

Skoug, R. M., et al., Upstream and magnetosheath energetic ions with energies to approximately $\approx$2 MeV, *Geophys. Res. Lett., 23*, 1223-1226, 1996.

Slavin, J. A., and R. E. Holzer, Solar wind flow about the terrestrial planets, 1, Modeling bow shock position and shape, *J. Geophys. Res., 86*, 11,401-11,411, 1981.

Slavin, J. A., R. E. Holzer, J. R. Spreiter, and S. S. Stahara, Planetary Mach cones: Theory and observation, *J. Geophys. Res., 89*, 2708-2714, 1984.

Spreiter, J. R., and S. S. Stahara, Magnetohydrodynamic and gasdynamic theories for planetary bow waves, in *Collisionless Shocks in the Heliosphere: Reviews of Current Research, Geophys. Monogr. Ser.*, vol. 35, edited by B. T. Tsurutani and R. G. Stone, pp. 85-107, AGU, Washington, D. C., 1985.

Terasawa, T., Origin of 30 $\sim$ 100 keV protons observed in the upstream region of the Earth's bow shock, *Planet. Space Sci., 27*, 365-384, 1979.

Winglee, R. M., et al., Modeling of upstream energetic particle events observed by WIND, *J. Geophys. Res., 23*, 1227-1230, 1996.

T. J. Freeman, Space Sciences Laboratory, University of California, Berkeley, CA 94720-7450. (freeman@ssl.berkeley.edu)

G. K. Parks, Geophysics Program, University of Washington, Seattle, WA 98195-1650.

(Received June 14, 1999; revised October 26, 1999; accepted December 6, 1999.)